NTNU
Kunnskap for en bedre verden

Department of Engineering Cybernetics

TTK4250 - Sensor Fusion

Graded Assignment 1

Group 1
Finn Gross Maurer
Magnus Hellebust Haaland
Tarek El-Agroudi

Word count: 1158
November, 2022

1 Simulated data

1.1 The covariance of the orientation error

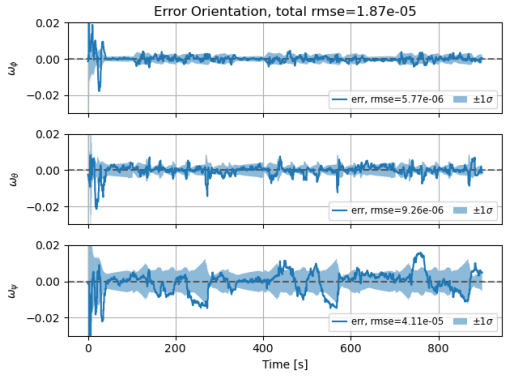

Figure 1: Error in orientation for simulated data with default parameters.

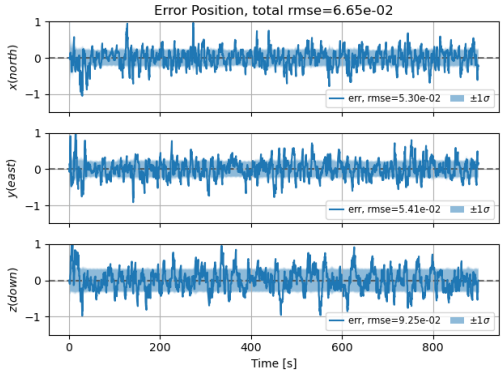

Figure 2: Error in position for simulated data with default parameters.

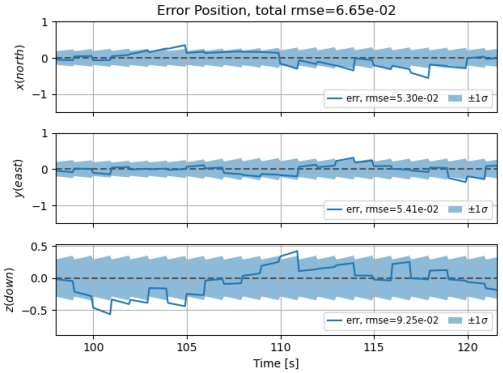

Figure 3: Magnified error in position for simulated data with default parameters.

Comparing the estimation errors for orientation and position, in figures 1 and 2, we see that the covariance of the estimated orientation error varies a lot more. While both display the classic "ramp-reset" effect of the prediction and correction steps of the Kalman filter, this effect is much more uniform for the position error (figure 3). The difference between the correction sizes in orientation indicates that each GNSS measurement does not update the estimate equally much.

Position is trivially observable from a GNSS measurement. For orientation however, Hong [4] showed that for constant acceleration, the attitude, and the gyro bias in the direction of the specific force, are unobservable. This means that we only can get significant updates from the GNSS when the UAV has undergone sufficient maneuvering [4].

1.2 The yaw error

Since the UAV mostly is level, the specific force mostly coincides with the body z axis such that it is the gyro bias in yaw that most often becomes unobservable. If it is unobservable, the ESKF will naturally not be able to update it from GNSS measurements. This could cause the increased error of yaw relative to pitch and roll.

The estimated error does not diverge because there is sufficient maneuvering, and enough non-level flight for the attitude and the yaw gyro bias to be observable sometimes. Notice from figure 4 that when we have non-level flight the observability of other gyro biases becomes worse. For instance,

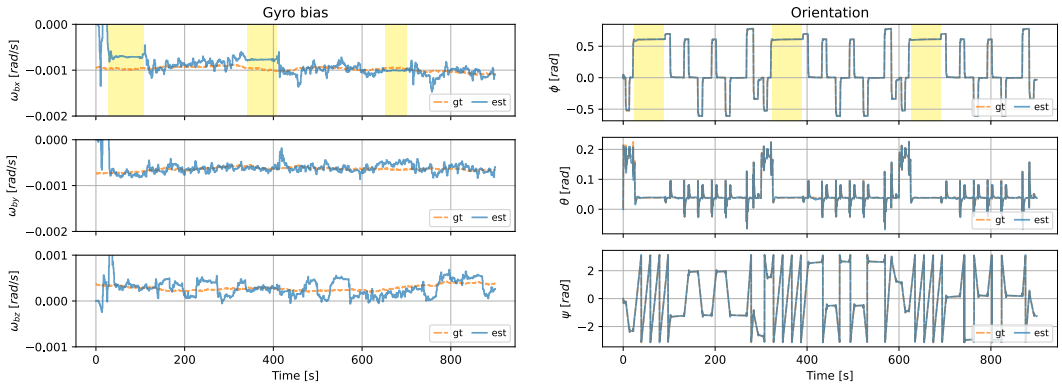

Figure 4: Gyro bias and orientation for simulated data with initial parameters. The yellow boxes shows the connection between roll angle and the observability of the x component of the gyro bias.

when there is significant roll for prolonged time, we see that the x bias becomes unobservable, as is highlighted in yellow.

The only case were the true error will not diverge for a constant-acceleration UAV, for instance a stationary one, is if the bias in the specific force direction is by chance set to the correct value.

1.3 Rounding of correction matrices

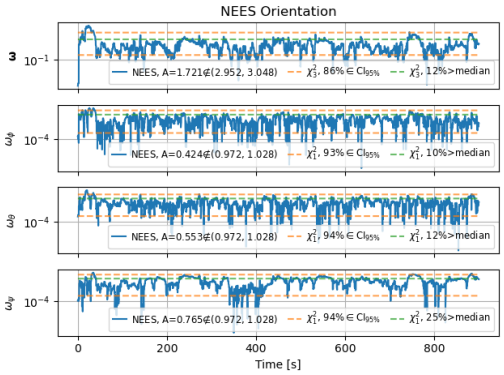

Figure 5: NEES in orientation for simulated data with default correction matrices.

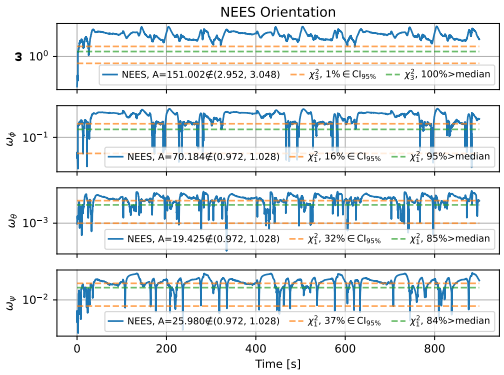

Figure 6: NEES in orientation for simulated data with rounded correction matrices.

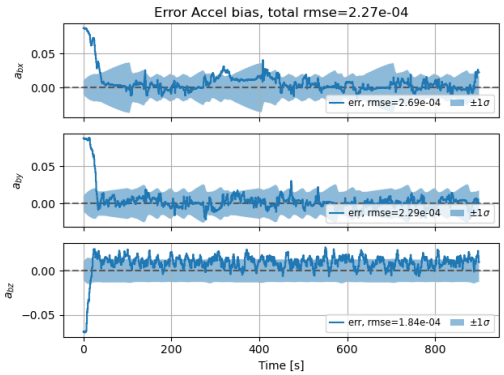

Figure 7: Error in acceleration bias for simulated data with default correction matrices.

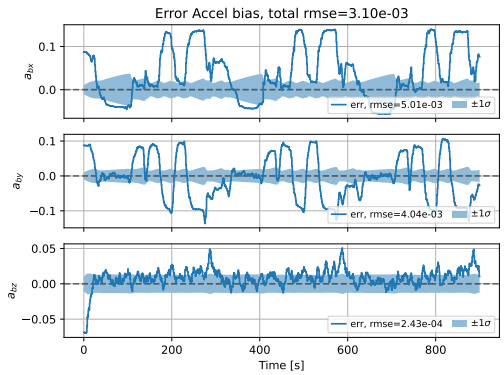

Figure 8: Error in acceleration bias for simulated data with rounded correction matrices.

The RMSE increases significantly from 1.87×10^{-5} and 6.65×10^{-2} for the orientation error and position errors before rounding, to 5.80×10^{-4} and 1.69×10^{-1} after. The degraded performance is further confirmed by the NEES in figures 5 and 6. We see that the NEES for the rounded case is significantly above the χ^2 limits, indicating an overconfident estimate [1]. This makes sense, because less accurate IMU measurements increase the model error.

Furthermore, when we study the bias errors for the non-rounded and rounded correction matrices, plotted in figures 7 and 8 respectively, we notice how we have severe consistency issues in the rounded case. The true error in the bias sometimes shoots far out of the covariance region. This occurs because the biases account for the errors in the correction matrices if the UAV maintains its attitude for a while in a way that *depends on the attitude*. The spikes occur when the UAV suddenly changes its attitude such that the bias has grown in the wrong direction.

1.4 Tuning

1.4.1 NEES tuning of orientation

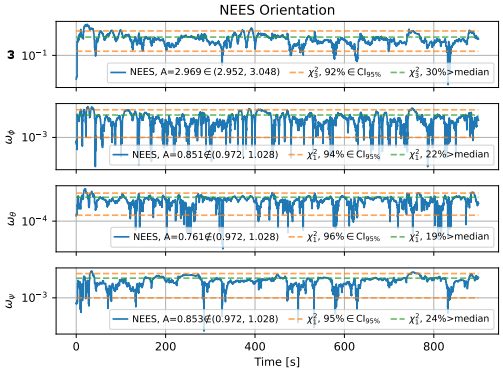

Figure 9: NEES in orientation for simulated data with noise parameters given in table 1.

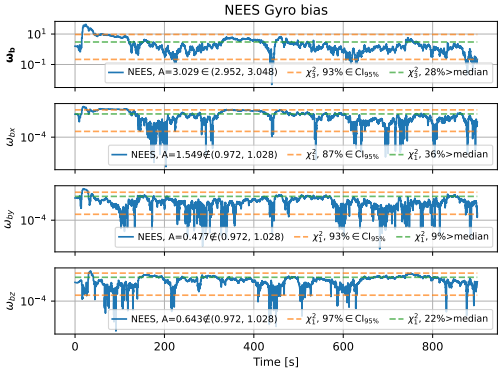

Figure 10: NEES in gyro bias for simulated data with noise parameters given in table 1.

Table 1: Standard deviation for gyro and gyro bias noise.

	SD parameter	
Parameter	Old value	New value
Gyro	4.36×10^{-5}	9×10^{-6}
Gyro bias	5×10^{-5}	9×10^{-6}

Table 2: RMSE values for orientation and gyro bias.

	RMSE	
State	Old value	New value
Orientation	1.87×10^{-5}	9.86×10^{-6}
Gyro bias	5.00×10^{-8}	3.98×10^{-8}

We seek an "optimal" configuration for the orientation estimate, with an RMSE error as small as possible and a NEES overall inside the χ^2 bounds. The results of some manual tuning are shown in figures 9, 10. The main change involved a decrease in the standard deviation of the noise of both the gyrometer and gyrometer bias. This was done because the NEES in general was below the χ^2 bounds. As can be seen in table 2, this also yields slightly better RMSE values.

1.4.2 Initial orientation

For a real drone, the initial roll and pitch can be estimated through accelerometer leveling [2, sec. 14.2.1]. This is not so for the yaw angle due to the observability issues discussed in 1.1. Figure 11 shows the orientation trajectory for the filter when the initial orientation is offset by 180 degrees in yaw. Convergence to the correct attitude now takes over 125 seconds. The slower convergence can be attributed to the violation of the small-angle asumption for the representation of the quaternion error in the ESKF [1, sec. 10.3.3], rendering the approximation inaccurate.

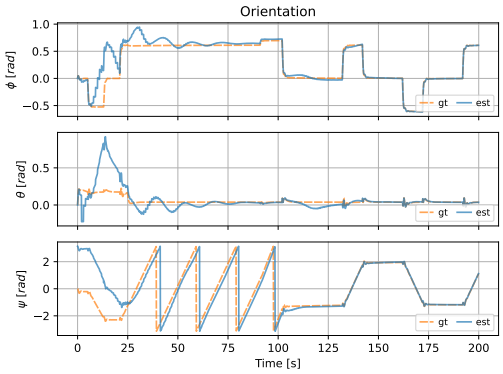

Figure 11: Orientation for simulated data with initial yaw angle off by 180 degrees.

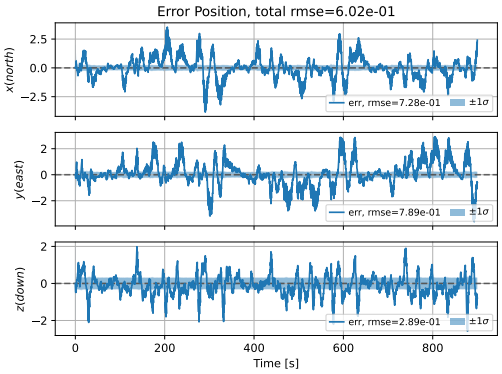

Figure 12: Error in position for simulated data with IMU running on 10 Hz.

1.4.3 Reduced IMU measurement frequency

Figure 12 shows the estimation error in position when the IMU measurements arrive at a frequency of 10 Hz instead of the default case of 100 Hz. The RMSE for position is now 60 cm, which represents an increase by a factor 10. This is because the prediction step now involves integrating an acceleration over a much longer time step. In particular, the approximation that the acceleration is constant over the time step becomes worse.

2 Real data[1]

2.1 Handling GNSS timing

To ensure temporal consistency between prediction and correction, we can set the prediction length to the time between the previous time step and the GNSS measurement time. Furthermore, due to the causality of IMUs [3], one should use the next IMU measurement for this prediction.

In practice, upon receiving a GNSS measurement, we wait for an IMU measurement, use it to predict the state at the GNSS measurement time, run the standard correction, injection and reset, and store the resulting states for the next iteration.

2.2 Rounding of correction matrices

Figure 13 shows that the NIS only is increased when the gyrometer and accelerometer corrections are rounded individually and not together. It is therefore hard to provide conclusive evidence on the IMU's calibration from only the position NIS.

Looking at the the bias estimates in figures 7 and 8, we can identify spikes in both cases which could be a result of poor correction. Note that these occur both before and after rounding, which could indicate that the IMU was not corrected particularly well in the first place. However, the spikes could also originate from an incorrect gravity vector (section 2.3.3), and we have no way of seeing this directly from the results.

The uncertainty in the conclusions demonstrates the importance of setting up the correction matrices thoroughly or to estimate these online.

[1]Disclaimer: We hypothesize that the data was already corrected with respect to IMU rotation before the correction in the code. Because the IMU has been corrected twice, the new "body frame" now has a y axis aligned with the front of the plane. If, as we assume (see section 2.3.2), the initial orientation and lever arm are given in classical body NED, this becomes wrong. We compensated for the initial orientation by increasing the initial yaw by 90 degrees. We did not compensate for the wrong lever arm.

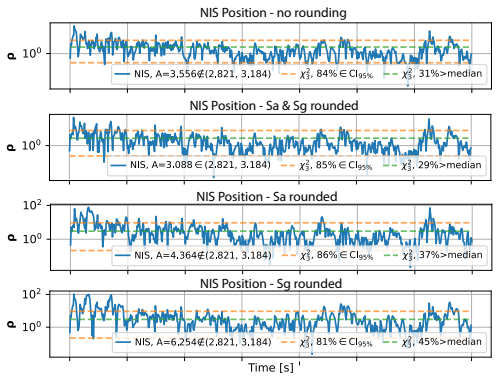

Figure 13: Acceleration bias for real data with rounded correction matrices.

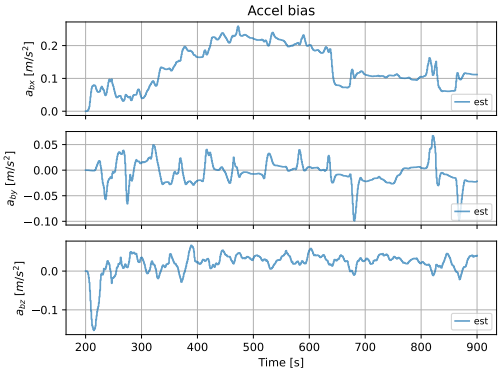

Figure 14: Acceleration bias for real data with default parameters.

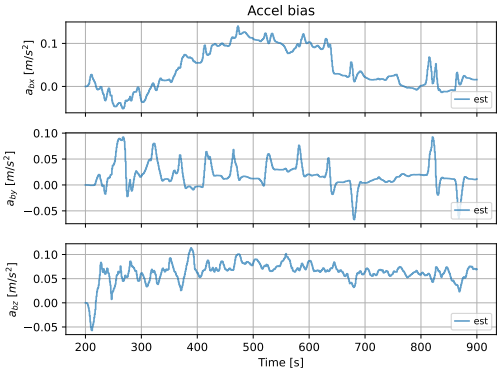

Figure 15: Acceleration bias for real data with both rounded correction matrices.

2.3 Tuning

2.3.1 Tuning from NIS

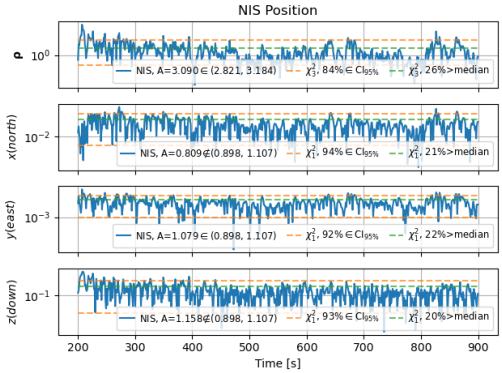

Figure 16: NIS in position for real data after tuning.

With real data, we only have the NIS for the position measurement. The problem with this is that, while a wellbehaved NIS could indicate a good position estimate, it does not *directly* tell us anything about orientation and the biases. Some initial tuning gives the NIS in figure 16, where the gyrometer and accelerometer standard deviation have been increased by a factor 10 in order to decrease the NIS from the non-rounding case in figure 13.

2.3.2 Initial orientation

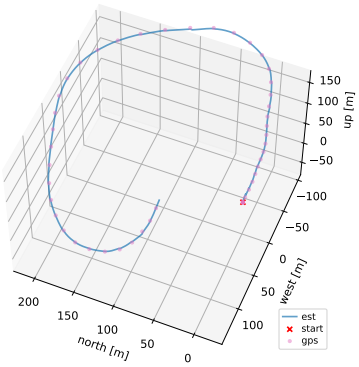

Figure 17: Position for real data with correct initial orientation.

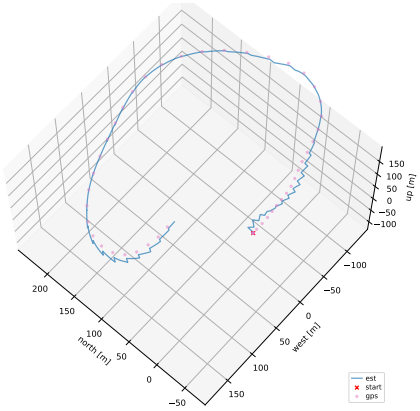

Figure 18: Position for real data with initial orientation off by 90 degrees.

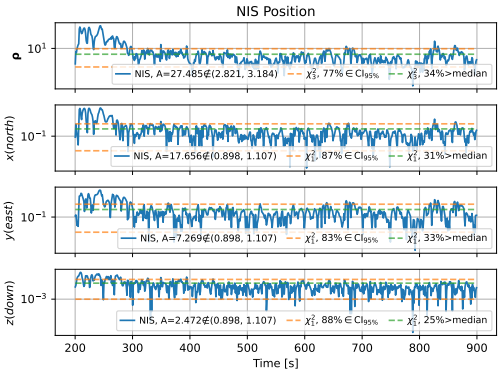

Figure 19: NIS in position for real data with initial orientation off by 90 degrees.

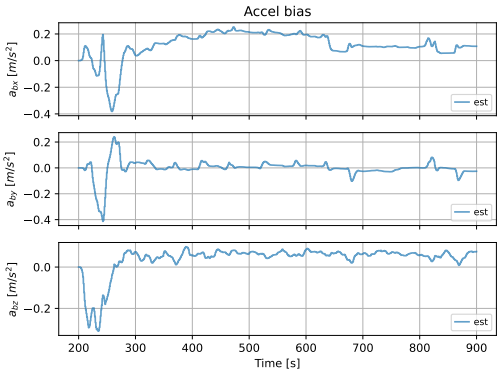

Figure 20: Acceleration bias for real data with corrected gravitational vector.

For a real system, we are unable to correctly initialise the yaw angle without additional sensors such as a magnetometer. One way to identify an incorrect initial orientation could be by comparing the estimated trajectory with the GNSS measurements for several initialisations. This was done for initial yaw angles 180 and 90 degrees in figures 18 and 17, respectively. It is obvious from the discrepancy between measurment and estimates that the 180 degrees case is a better initial yaw. This is confirmed by looking at the NIS in figure 19, which is much higher for the early trajectory in the case of wrong initial orientation.

2.3.3 Tuning the gravity vector

As mentioned in section 2.2, the spikes in acceleration bias can also originate from an incorrect gravity vector. A faulty gravity vector will give an error component in the other accelerometer components, which will vary based on attitude, and be compensated for by the biases.

In [5], the actual gravity vector at the flight location was specified to be $\mathbf{g^n} = [-0.02639, -0.00916, 9.85573]^\top$. Running the data with this gives the acceleration biases in figure 20, where we clearly see that the spikes from before have almost disappeared!

Bibliography

[1] Edmund Brekke. *Fundamentals of Sensor Fusion*. 3rd ed. 2022.

[2] Thor I. Fossen. *HANDBOOK OF MARINE CRAFT HYDRODYNAMICS AND MOTION CONTROL*. 2nd ed. 2021.

[3] Emil Martens. *Graded Assignment 1*.

[4] S.Hong et al. 'Observability of Error States in GPS/INS Integration'. In: *IEEE TRANSACTIONS ON VEHICULAR TECHNOLOGY* 54 (2005).

[5] Martin Lysvand Sollie. 'Estimation of UAV Position, Velocity and Attitude Using Tightly Coupled Integration of IMU and a Dual GNSS Receiver Setup'. In: *NTNU, Department of Engineering Cybernetics* (2018). URL: https://ntnuopen.ntnu.no/ntnu-xmlui/handle/11250/2561061.